OPEN

High-performance transparent and stretchable all-solid supercapacitors based on highly aligned carbon nanotube sheets

Tao Chen[1], Huisheng Peng[2], Michael Durstock[3] & Liming Dai[1]

[1]Center of Advanced Science and Engineering for Carbon (Case4Carbon), Department of Macromolecular Science and Engineering, Case Western Reserve University, 10900 Euclid Avenue, Cleveland, OH 44106 (USA), [2]State Key Laboratory of Molecular Engineering of Polymers, Department of Macromolecular Science and Laboratory of Advanced Materials, Fudan University, Shanghai 200438, China, [3]Materials and Manufacturing Directorate, Air Force Research Laboratory, RXBP, Wright-Patterson Air Force Base, OH 45433, USA.

By using highly aligned carbon nanotube (CNT) sheets of excellent optical transmittance and mechanical stretchability as both the current collector and active electrode, high-performance transparent and stretchable all-solid supercapacitors with a good stability were developed. A transmittance up to 75% at the wavelength of 550 nm was achieved for a supercapacitor made from a cross-over assembly of two single-layer CNT sheets. The transparent supercapacitor has a specific capacitance of 7.3 F g^{-1} and can be biaxially stretched up to 30% strain without any obvious change in electrochemical performance even over hundreds stretching cycles.

Transparent energy conversion and storage devices have attracted increasing attentions recently due to their great potentials as integrated power sources for displays and windows, for example, for buildings, automobiles and aerospace vehicles[1–6]. On the other hand, it is highly desirable to have energy conversion and storage devices not only transparent but also mechanically stretchable for many other applications, ranging from self-powered rolled-up displays to self-powered wearable optoelectronics[7–12]. While a transparent supercapacitor is often necessary for power-integrated devices to be both functional and aesthetic appeal, for example, for windows of buildings, automobiles and aerospace vehicles[5,6], its stretchability can ensure a stable performance even under unpredictable mechanical deformations (e.g., bending, stretching)[10–12]. Highly stretchable electronics have opened up exciting opportunities for the development of large-area, light-weight and wearable electronics. Like other stretchable optoelectronic units (e.g., organic solar cells, light-emitting diodes, and field effect transistors)[13–15], transparent and stretchable supercapacitors are one of the critical components in power-integrated flexible optoelectronic systems. However, it remains a great challenge to develop both transparent and stretchable supercapacitors because most of the existing electrodes are neither stretchable nor transparent (e.g., metal electrodes) with some of them either stretchable of a low transmittance (e.g., conducting polymers) or transparent of a low stretchability (e.g., ITO, other metal oxides). To our best knowledge, no optoelectronic or energy-related device has been reported to date to show both good transparency and high stretchability, though many devices with only one function have been reported elsewhere[1–6,13–16].

Owing to their excellent electrical, optical and mechanical properties, carbon nanomaterials, including carbon nanotubes (CNTs) and graphene sheets, have been widely used as active materials in supercapacitors[17–21]. They have also been used as transparent or stretchable conductive electrodes[22–29]. Thus, these earlier studies have demonstrated that carbon nanomaterials are promising for the development of transparent and stretchable power-integrated optoelectronic devices, including transparent and stretchable supercapacitors. However, no such a supercapacitor has been devised, presumably owing to technical difficulties in producing/handling the optically thin, but mechanically strong, electrodes. Herein, we report the first transparent and stretchable all-solid supercapacitor, in which aligned carbon nanotube (CNT) thin sheets were used as both the current collector and active material with polydimethylsiloxane (PDMS) as the transparent and stretchable substrate. The supercapacitors newly-developed from a cross-over assembly of two single-layer CNT sheets showed a transmittance up to

75% at the wavelength of 550 nm and a specific capacitance of 7.3 $F g^{-1}$, comparing favorably with the value of 6.4 $F g^{-1}$ previously reported for transparent supercapacitors based on the bare CNT electrode[16]. They can be biaxially stretched up to 30% strain without any obvious change in electrochemical performance even over 100 stretching cycles.

Results

Figure 1a schematically shows the procedures for preparing the transparent and stretchable supercapacitors. To start with, we synthesized a highly aligned multiwalled CNT forest (Figures S1 and 2b) through chemical vapor deposition of ethylene onto a silicon wafer pre-coated with Fe (1.2 nm)/Al_2O_3 (3 nm) under a mixture of argon and hydrogen (flow rate of 400 sccm/30 sccm) as the carrier gas at $750°C$[23–25]. Following the reported method[23,25], we then continuously drew a transparent CNT sheet out from the CNT forest onto a pre-formed PDMS substrate (Figures 1a, 2a and 2c), followed by coating a solution of polyvinyl alcohol (PVA) and H_3PO_4 on the CNT sheet (Figure 1a). Finally, we constructed the supercapacitors by assembling another PDMS-supported CNT electrode on top of the newly-formed PVA-H_3PO_4/CNT/PDMS multilayer film in either a parallel (Figure 1b) or cross (Figure 1c) configuration, leading to highly transparent devices to be seen through even with the naked eye (Figures 1b and 1c). The resultant supercapacitors are also flexible and stretchable characteristic of the PDMS-supported aligned CNT sheets. The whole device can be bent, folded, and even stretched at least up to 30% strain (Figures 1d and 1e) without any obvious performance change, as we shall see later.

As shown in Figures 2a–c, the as-prepared vertically-aligned CNTs (Figure 2b) became horizontally-aligned along the drawing direction on the PDMS substrate (Figure 2c). However, there was no change in the structure and property (*e.g.*, specific surface area, electrical conductivity, mechanical strength) for each of the constituent nanotubes, though droplets of ethanol were used to enhance the CNT-PDMS contact. Raman spectrum of the PDMS-supported CNT sheet (Figure S2) shows a relatively low intensity ratio of the D-band to G-band (~0.4), indicating a high graphitization degree. The transmittance of a single-layer CNT sheet on the PDMS substrate (1 mm thickness with 92% transparency, as shown in Figure S3) is about 78% at the wavelength of 550 nm, which decreased to 68% and 58% for the corresponding two- and three-layer CNT sheets, respectively (Figure 2d). As seen in Figure S3, the optical transmittance of a CNT sheet on the PDMS substrate almost unchanged even after having been stretched up to 100 times, suggesting an excellent optical stability and stretchability. By carefully fixing

the PDMS-supported CNT electrode on a micro tensile test machine (MV220 Motorized Test Stand, DS2-11 Digital Force Gauge; IMADA, Inc.), we have also investigated the resistance dependence on the tensile strain for the CNT sheet with and without PVA coating. As shown in Figure 2e, the resistance of the bare CNT sheet increased by 350% with 30% increase in tensile strain upon stretching the electrode along the nanotube length direction. The increased resistance can be attributed to the stretching-induced nanotube-nanotube contact loss, as schematically shown in Figure S4a. In contrast, the transverse stretching of the same CNT sheet up to 30% tensile strain led to only about 40% increase in resistance. This is because, in this particular case, the nanotube network could show lateral expansion without the nanotube-nanotube contact loss (Figure S4b). Upon coating a layer of PVA (thickness of about 50 μm as the electrolyte) onto the CNT sheet and stretching it up to 30% tensile strain along and perpendicular to the nanotube length direction, the resistance of the PVA-coated CNT sheet was found to increase by only 80% and 40%, respectively (Figure 2e). The improved stretchability induced by the PVA confinement is an additional advantage for the use of the PVA-coated CNT electrode in the transparent and stretchable supercapacitors to be developed in this study.

Supercapacitors with different optical transmittances could be fabricated by using the transparent electrode with different layers of CNT sheets on the PDMS substrate. When a single-layer CNT sheet on the PDMS substrate was used as the transparent electrode, the resultant supercapacitor showed a high transparency (Figure 3a) and a high flexibility, which could be easily bent or even folded into any angle without any obvious detrimental effect on the device performance (Figures 3a and 3b). More specifically, a parallelly assembled supercapacitor with two transparent electrodes, each with one layer of CNT sheet on the PDMS substrate, showed about 64% transmittance at the wavelength of 550 nm (Figure 3c). This value of transmittance is slightly lower than the corresponding transmittance for a single electrode with two layers of CNT sheets (68%, see Figure 2d; the black curve in Figure 3c refers to a single layer CNT sheet supported by the PDMS substrate with an overall transmittance of 78%) due to the presence of the polymer (PVA) electrolyte and another layer of the PDMS substrate in the device assembly. However, the corresponding supercapacitor assembled with a crossover configuration showed 75% transmittance at 550 nm (Figure 3c), a value which is higher than that of the parallelly–assembled device due to reduced CNT overlapping in the former. Like CNT sheets on the bare PDMS substrate, the optical transmittance of the assembled supercapacitors decreased with increasing layer number of the CNT
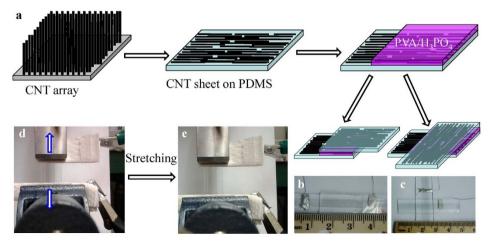

Figure 1 | **Schematics of the fabrication process for the transparent supercapacitors and their optical images.** (a) Schematic illustration of the process for fabricating the transparent and stretchable supercapacitor. (b, c) Photographs of supercapacitors assembled in the parallel and cross configurations. (d, e) Photographs of a supercapacitor before and after stretching.
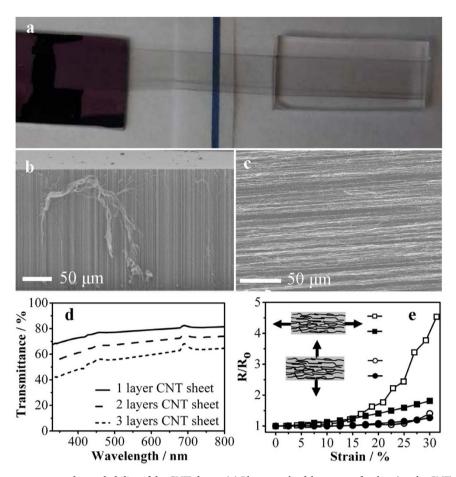
Figure 2 | Morphology, transparency and stretchability of the CNT sheets. (a) Photograph of the process for drawing the CNT sheet from the CNT forest onto a PDMS substrate. (b) SEM image of the CNT forest vertically aligned onto the silicon substrate. The misalignment seen for some of the carbon nanotubes was caused by peeling action during the SEM sample preparation. (c) SEM image of the as-prepared horizontally aligned CNT sheet. (d) Transmittance spectra of the PDMS substrates coated with different layers of the CNT sheet. (e) Normalized resistance of a bare CNT sheet on the PDMS substrate as a function of tensile strain, the CNT sheet before (open square) and after (solid square) coating with PVA being stretched parallelly along the nanotube length direction, and the CNT sheet before (open circle) and after (solid circle) coating with PVA being stretched in a normal direction to the nanotube length.

sheets on the transparent electrode. Indeed, the transmittance of the parallelly-assembled supercapacitors reduced from 64% to 35% at 550 nm as the CNT layer number on each of the two transparent electrodes increased from one to three (Figure S5). Similarly, the assembled supercapacitors also showed a good optical stability with a small transmittance change (<2%) even after having been stretched 100 times (Figure S3).

Figure 3d shows the cyclic voltammetry (CV) curves recorded at a scan rate of 0.1 V s^{-1} for the transparent supercapacitors assembled in a parallel and cross configuration, respectively. As can be seen, both of the devices showed good electrochemical stability and capacitive behaviors at scan rates from 0.05 to 1.0 V s^{-1} (Figures S6 and S7). The capacitance of device (C_T) can be calculated by using the voltammetric charge integrated from the CV curve according to Equation (1)[30–32],

$$C_T\left(\text{F g}^{-1}\right) = \frac{1}{2mVv}\int_{V_-}^{V_+} I(V)\mathrm{d}V \qquad (1)$$

where m is the mass of the active materials in both electrodes, V ($= V_+ - V_-$) is the potential window between the positive and negative electrode, v (V s^{-1}) is the scan rate. The specific capacitance of the cross-assembled supercapacitor can thus be calculated to be 3.8 F g^{-1} at 0.1 V s^{-1}, which was 47% higher than that (2.6 F g^{-1}) of the parallelly assembled device (Figures S6b and S7b). At a constant scan rate v, the average specific power density (P, in W kg^{-1}) during

discharge can be calculated by integrating CV curves using equation (2)[30–32],

$$P = \frac{1}{Vm}\int_0^{V_+} IV\mathrm{d}V \qquad (2)$$

where V is the initial voltage during discharge and the m is the total mass of both electrodes. The specific energy density (E, in Wh kg^{-1}) can be calculated according to equation (3),

$$E = \frac{1}{3600vm}\int_0^{V_+} IV\mathrm{d}V \qquad (3)$$

The specific power density and energy density of cross-assembled supercapacitor at the scan rate of 0.1 V s^{-1} were found to be 1.1 kW kg^{-1} and 1.0 Wh kg^{-1}, respectively, both of which are slightly higher than those of the parallelly assembled device (Figure S6c and S7c).

Galvanostatic charge/discharge curves with a nearly triangular shape shown in Figure 3e for both of the supercapacitors with a parallel and crossover configuration indicated, once again, the good capacitive behavior with a high Coulombic efficiency as well as no obvious IR drop. The specific capacitance of a supercapacitor can be calculated from the equation of $C = I/m(-\Delta V/\Delta t)$, where I is the applied current, m is the mass of active materials at both electrodes, $\Delta V/\Delta t$ is the slope of discharging curve[30–32]. In order to avoid over-estimating of the specific capacitance, $\Delta V/\Delta t$ was calculated from the
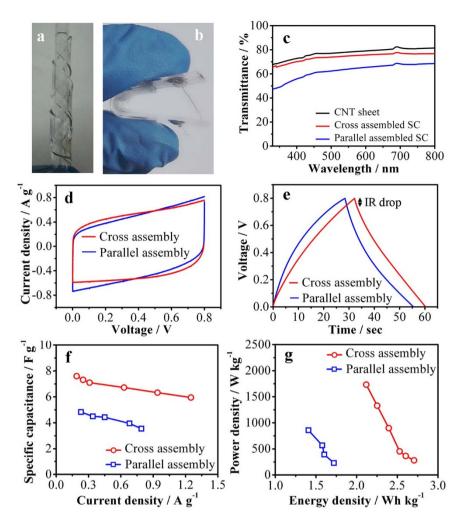
Figure 3 | The optical and electrochemical properties of the transparent supercapacitors based on the transparent and stretchable electrodes with one layer of CNT sheet on the PDMS substrate. (a) A photograph of such a supercapacitor wrapped outside along a glass tube. (b) A photograph of a bended transparent supercapacitor based on the transparent electrodes with one layer CNT sheet. (c) Transmittance spectra of one layer CNT sheet on PDMS substrate and its derived supercapacitors with different assembled configurations. (d) Cyclic voltammetry curves of the supercapacitors at a scan rate of 0.1 V s^{-1}. (e) The galvanostatic charging-discharging curves of the supercapacitors at a constant current density of 0.25 A g^{-1} for the parallel assembly and 0.23 A g^{-1} for the cross assembly. (f) Dependence of specific capacitance of devices on the discharging current density for both types of devices. (g) Ragone plots of the both types of supercapacitors.

equation of $\Delta V/\Delta t = (V_2 - V_1/2)/(T_2 - T_1)$, where V_2 and V_1 are the potential after IR drop and the half potential of the discharge curve, respectively, T_2 and T_1 are the corresponding discharge time of V_2 and V_1[31–33]. From Figure 3e, the specific cell capacitance was determined to be about 7.3 F g^{-1} for the cross assembled supercapacitor under the discharge current of 0.25 A g^{-1}, much high than that (4.9 F g^{-1}) of the parallelly assembled device under the discharge current of 0.23 A g^{-1}. This value is slightly better than that (6.4 F g^{-1}) previously reported for transparent supercapacitors based on only CNTs electrode but lower than that of the same device after improved by conductive polymer with the pseudocapacitive effect[16]. Therefore, there is large space to further improve the performance of this type supercapacitors. The specific capacitance of a single electrode was obtained by multiplying the C by four, which is about 29.2 F g^{-1} for the cross-assembled supercapacitor, slightly better than the value of 27.5 F g^{-1} previously reported for transparent supercapacitors[18]. The specific capacitance for both type supercapacitors decreased as the current density increased (Figure 3f), indicating a high series resistance associated with the thin CNT sheet and the inefficient contact among the constituent CNTs. Figure 4g shows the corresponding Ragone plots, in which the energy density (E) and power density (P) were calculated according to the following

equations, E (Wh kg^{-1}) $= 0.5CV^2*1000/3600$ and P (W kg^{-1}) $= 3600$ E/t, where t is the discharge time[32–35]. An energy density of 2.4 and 1.4 Wh kg^{-1} was obtained for the cross and parallel assembly, respectively, with a power density of ~0.9 kW kg^{-1} for both devices (specific capacitance of 6.7 F g^{-1} at the current density of 0.63 A g^{-1} for the cross assembly and 4.0 F g^{-1} at 0.34 A g^{-1} for parallel assembly). The obtained energy density is comparative with that of the flexible supercapacitor based on In$_2$O$_3$ nanowire/carbon nanotube heterogeneous films[36]. All of the cell capacitance, specific power and energy densities calculated from both methods described above are comparative. Unlike conventional supercapacitors using metal (e.g., copper and gold) current collectors, we used carbon nanotubes as both current collector and active materials at present work in order to obtain stretchable and transparent devices. The high contact resistance among carbon nanotubes made the resultant supercapacitors with a relatively high series resistance, leading to a quick decrease in the power and energy densities with increasing the charging current density. The performance for supercapacitors based on the electrodes with two and three CNT layers, respectively, has also been investigated. Figure S8 shows CV curves and galvanostatic charge-discharge curves of these devices. Both of them also showed good electrochemical stability and capacitive behaviors. The specific capacitance
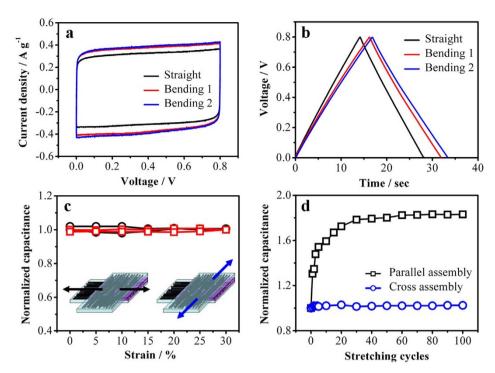
Figure 4 | Flexibility and stretchability of the transparent supercapacitors. (a) CV curves (at the scan rate of 0.1 V s^{-1}), and (b) the galvanostatic charge-discharge curves (with a constant current density of 0.20 A g^{-1}) of the supercapacitor with electrodes based on one-layer CNT sheet on the PDMS substrate under different states. (c) Normalized specific capacitance of the supercapacitor with cross assembly as a function of tensile strain as it was biaxially stretched. (d) Normalized specific capacitance of two type supercapacitors as a function of stretching cycles.

decreased from 7.3 F g^{-1} for the supercapacitor based on the one-layer CNT electrodes to 3.2 and 2.3 F g^{-1} as the CNT layer number increased to two and three, respectively. The observed inversely proportional relationship between the specific capacitance and the CNT layer number could be attributed to the fact that the active sites per unit mass of the nanotube electrodes decrease as the CNT layer number increases due to the interlayer nanotube overlapping.

Electrochemical impedance spectroscopy (EIS) is a powerful tool to understand the electrochemical behaviors at the bulk and interface of supercapacitors[37,38]. Figures S6d and S7d showed the Nyquist plots of supercapacitors with cross and parallel assembly, respectively, in the frequency ranging from 10^{-2} to 10^5 Hz. The Nyquist plots was fit well to an equivalent circuit as shown in the inset of Figure S6b and S7b by the equation (4),

$$Z = R_S + \frac{1}{j\omega C_{DL} + \dfrac{1}{R_{CT} + W_O}} - \frac{j}{\omega C_F} \quad (4)$$

where R_S is the series resistance, C_{DL} is double-layer capacitance, R_{CT} is charge transfer resistance, W_O is the Warburg diffusion element, and C_F is the faradic capacitance. Typically, the Nyquist plot of a supercapacitor can be divided into three regions according to the range of frequency. At high frequency, the intersection point on the real axis reveals the ohmic resistance of the electrolyte and the internal resistance of the electrode, termed as series resistance (R_S). From Figures S6b and S7b, series resistances of supercapacitors with parallel and crossover configurations are 2820 Ω and 930 Ω, respectively. The high R_S will reduce the ion and charge transport, leading to limited capacitance. To realize stretchable and transparent devices, no metal current collector was used, and hence the observed high series resistance. Therefore, the observed high R_S in the present study was mainly ascribed to the relatively high resistance of CNTs with a low packing density and poor contact associated with the very thin aligned CNT sheet. As shown in Figure S9, the R_S decreased from 2820 Ω to 790 Ω and 920 Ω as the layer number of CNT sheet

increased from one to two and three, respectively, suggesting that the high R_S is mainly associated with the intertube resistance within the CNT sheet, particularly over two layers. Therefore, the R_S can be decreased and performance of the device would be enhanced if conductive polymers were introduced to increase connections of the isolated CNTs within the CNT sheet. The semicircular behavior in the high-to mid-frequency region of a Nyquist plot represents the parallel connection of the interfacial charge transfer resistance (R_{CT}) and double-layer capacitance (C_{DL}). The transition from the semicircle to the long tail is attributed to the ion diffusion inside the electrolyte. At low frequency, the straight line vertical to real axis comes from an ideally polarizable capacitance, which can be seen in all of Nyquist plots in Figure S9, suggesting these devices with good capacitive behaviors.

Discussion

To evaluate the flexibility of the transparent supercapacitors, cyclic voltammetric and galvanostatic charging-discharging measurements were performed under mechanical deformations, including bending and stretching. Figure 4a shows typical CV curves of a transparent supercapacitor at straight and bending states. It is interesting to note that larger rectangular CV curves were obtained when the supercapacitor was under bending, so are the specific capacitance deduced from the charging-discharging curves (Figure 4b). Both could be ascribed to a bending-induced decrease in distance between the two electrodes.

CV and galvanostatic charging-discharging measurements were also performed on the supercapacitors when they were stretched to different strains. It was found that the specific capacitance of a parallelly assembled supercapacitor slightly increased by 33% as the tensile strain increased to about 30% by stretching along the nanotube length direction (Figure S10), and then leveled off as the stretching force was released. Figure S11 shows the corresponding CV and charge-discharge curves. However, it is difficult for the parallelly assembled supercapacitor to be stretched in the direction normal to the nanotube length as the transversely stretching could easily

destroy the device. In contrast, the supercapacitor with a cross assembly configuration showed a good stability even during a biaxial stretching process. Figure S12 shows the CV and charge-discharge curves recorded for a supercapacitor with the cross assembly when it was stretched up to the strain of 30% in both directions (Figure 4c), revealing an almost constant specific capacitance. This is because the transversely stretching could cause lateral expansion of the nanotube network, but almost without the nanotube-nanotube contact loss along the nanotube length direction (Figure S4b). Unlike most of the stretchable supercapacitors reported previously[10–12], our devices are not only both transparent and stretchable but also can be biaxially stretched with an excellent electrochemical stability over many stretching cycles (Figure 4d). For comparison, the parallelly assembled supercapacitor showed an over 70% increase in capacitance during initial twenty stretching cycles before reaching a stable capacitance. This capacitance increase with the stretching cycles could be attributed to the combined effects associated with the stretching-induced increase in the active sites of the CNT sheet and loss of the nanotube-nanotube contacts (cf. Figure S4a). Both types of the supercapacitors showed a good stability even after hundreds of stretching cycles, exhibiting great potential for practical applications.

In summary, we have, for the first time, demonstrated that transparent and stretchable all-solid supercapacitors could be developed using aligned CNT sheet(s) on a PDMS substrate as the transparent (up to ~80%) and flexible current collector and active materials, followed by pasting the two PDMS-supported CNT electrodes tightly together with A PVA-H_3PO_4 gel electrolyte. Supercapacitors thus prepared with a cross assembly of two transparent electrodes, each of them with one layer CNT sheet on the PDMS substrate, showed an optical transmittance up to ~75% at the wavelength of 550 nm and a specific cell capacitance of 7.3 F g^{-1}, outperformed previously-reported transparent supercapacitors (6.4 F g^{-1}). Furthermore, our transparent supercapacitors also showed a high flexibility and stretchability with an excellent stability even under biaxial stretching for hundreds cycles. Therefore, these newly-developed transparent and stretchable all-solid supercapacitors are promising for various power-integrated stretchable optoelectronic systems.

Methods

Vertically aligned CNT forest was synthesized by chemical vapor deposition of ethylene as the carbon source using the sputter-coated Fe (1.2 nm)/Al_2O_3 (3 nm) catalyst on a silicon wafer as the nanotube growth substrate and a mixture of argon and hydrogen (flow rate of 400 sccm/30 sccm) as the carrier gas at 750°C[25]. The resultant vertically aligned CNT array was drawn into horizontally aligned CNT sheet onto a PDMS substrate, followed by dropping some ethanol droplets on the CNT sheet to enhance the contact between the CNT and the PDMS substrate. The surface specific density of the as-prepared single layer CNT sheet was measured at the range of 1.0 to 1.4 μg cm^{-2}, and the mass of CNT electrode was calculated by multiplying the density of CNT sheet and the effective area in supercapacitor. PDMS substrates with thickness about 1 mm were prepared by pouring the mixture of the "base" and the "curing agent" at a ratio of 10 : 1 (Sylgard 184, Dow Corning) into a rectangular molder, followed by thermally cured at 75°C for 1 h. Suitable shapes and sizes were cut from the cured piece. A gel containing poly(vinyl alcohol) powder (10 g) and H_3PO_4 (10 g) in water (100 mL) was used as the solid electrolyte. The gel electrolyte was coated over the most part (70% length) of the aligned CNT sheet (3–4 cm long and 0.4–1 cm wide) and dried in the air at room temperature for several hours. Then, two such electrolyte-coated CNT electrodes were assembled into a supercapacitor by pressing them together. Finally, the CNT sheet was connected with a copper wire using silver paste for subsequent characterization of the device performance.

The carbon nanotube structure was characterized by SEM (JEOL JSM-6510LV/LGS operated at 20 kV) and TEM (JEOL JEM-2100F operated at 200 kV). UV/Vis transmittance was measured on a Shimadzu UV1800 spectrometer while Raman spectra were recorded on a Renishaw Raman spectrometer equipped with 514-nm laser. Electrochemical measurements were performed on an electrochemical working station (CHI 760C, U.S.A.). The CNT sheet or supercapacitor was fixed on a mechanical test machine (MV220 Motorized Test Stand, DS2-11 Digital Force Gauge; IMADA, Inc.), the resistance or the electrochemical performance was measured under stretching and bending, respectively.

1. Huang, J. S., Li, G. & Yang, Y. A semi-transparent plastic solar cell fabricated by a lamination process. *Adv. Mater.* **20**, 415–419 (2008).

2. Chen, C.-C. *et al.* Visibly transparent polymer solar cells produced by solution processing. *ACS Nano* **6**, 7185–7190 (2012).

3. Görrn, P. *et al.* Towards see-through displays: fully transparent thin-film transistors driving transparent organic light-emitting diodes. *Adv. Mater.* **18**, 738–741 (2006).

4. Yang, Y. *et al.* Transparent lithium-ion batteries. *Proc. Natl. Acad. Sci. U.S.A.* **108**, 13013–13018 (2011).

5. Jung, H. Y., Karimi, M. B., Hahm, M. G., Ajayan, P. M. & Jung, Y. J. Transparent, flexible supercapacitors from nano-engineered carbon films. *Sci. Rep.* **2**, 773–777 (2012).

6. Niu, Z. *et al.* A repeated halving approach to fabricate ultrathin single-walled carbon nanotube films for transparent supercapacitors. *Small* **9**, 518–524 (2013).

7. Rogers, J. A., Someya, T. & Huang, Y. G. Materials and mechanics for stretchable electronics. *Science* **327**, 1603–1607 (2010).

8. Sekitani, T. *et al.* Stretchable active-matrix organic light-emitting diode display using printable elastic conductors. *Nat. Mater.* **8**, 494–499 (2009).

9. Lipomi, D. J., Tee, B. C.-K., Vosgueritchian, M. & Bao, Z. Stretchable organic solar cells. *Adv. Mater.* **23**, 1771–1775 (2011).

10. Yu, C., Masarapu, C., Rong, J., Wei, B. & Jiang, H. Stretchable supercapacitors based on buckled single-walled carbon-nanotube macrofilms. *Adv. Mater.* **21**, 4793–4797 (2009).

11. Xu, S. *et al.* Stretchable batteries with self-similar serpentine interconnections and integrated wireless recharging systems. *Nat. Commun.* **4**, 1543–1550 (2013).

12. Niu, Z. *et al.* Highly stretchable, integrated supercapacitors based on single-walled carbon nanotube films with continuous reticulate architecture. *Adv. Mater.* **25**, 1058–1064 (2013).

13. Kim, J. B. *et al.* Wrinkles and deep folds as photonic structures in photovoltaics. *Nat. Photonics* **6**, 327–332 (2012).

14. Yu, Z., Niu, X., Liu, Z. & Pei, Q. Intrinsically stretchable polymer light-emitting devices using carbon nanotube-polymer composite electrodes. *Adv. Mater.* **23**, 3989–3994 (2011).

15. Shin, G. *et al.* Stretchable field-effect-transistor array of suspended SnO_2 nanowires. *Small* **7**, 1181–1185 (2011).

16. Lin, H., Li, L., Ren, J., Cai, Z., Qiu, L., Yang, Z. & Peng, H. Conducting polymer composite film incorporated with aligned carbon nanotubes for transparent, flexible and efficient supercapacitor. *Sci. Rep.* **3**, 1353–1358 (2013).

17. Noked, M., Okashy, S., Zimrin, T. & Aurbach, D. Composite carbon nanotube/carbon electrodes for electrical double-layer super capacitors. *Angew. Chem. Int. Ed.* **51**, 1568–1571 (2012).

18. Hu, S., Rajamani, R. & Yu, X. Flexible solid-state paper based carbon nanotube supercapacitor. *Appl. Phys. Lett.* **100**, 104103 (2012).

19. Yu, D. & Dai, L. Self-assembled graphene/carbon nanotube hybrid films for supercapacitors. *J. Phys. Chem. Lett.* **1**, 467–470 (2010).

20. Jha, N., Ramesh, P., Bekyarova, E., Itkis, M. E. & Haddon, R. C. High energy density supercapacitor based on a hybrid carbon nanotube-reduced graphite oxide architecture. *Adv. Energy Mater.* **2**, 438–441 (2012).

21. El-Kady, M. F., Strong, V., Dubin, S. & Kaner, R. B. Laser scribing of high-performance and flexible graphene-based electrochemical capacitors. *Science* **335**, 1326–1330 (2012).

22. Wu, Z. *et al.* Transparent, conductive carbon nanotube films. *Science* **305**, 1273–1276 (2004).

23. Zhang, M. *et al.* Strong, transparent, multifunctional, carbon nanotube sheets. *Science* **309**, 1215–1219 (2005).

24. Zhang, Y. *et al.* Polymer-embedded carbon nanotube ribbons for stretchable conductors. *Adv. Mater.* **22**, 3027–3031 (2010).

25. Peng, H. Aligned carbon nanotube/polymer composite films with robust flexibility, high transparency, and excellent conductivity. *J. Am. Chem. Soc.* **130**, 42–43 (2008).

26. Zhang, X. *et al.* Spinning and processing continuous yarns from 4-inch wafer scale super-aligned carbon nanotube arrays. *Adv. Mater.* **18**, 1505–1510 (2006).

27. Liu, K. *et al.* Cross-stacked superaligned carbon nanotube films for transparent and stretchable conductors. *Adv. Funct. Mater.* **21**, 2721–2728 (2011).

28. Kim, K. S. *et al.* Large-scale pattern growth of graphene films for stretchable transparent electrodes. *Nature* **457**, 706–710 (2009).

29. Bae, S. *et al.* Roll-to-roll production of 30-inch graphene films for transparent electrodes. *Nat. Nanotechnol.* **5**, 574–578 (2010).

30. Lee, J. A. *et al.* Ultrafast charge and discharge biscrolled yarn supercapacitors for textiles and microdevices. *Nat. Commun.* **4**, 1971–1978 (2013).

31. Stoller, M. D. & Ruoff, R. S. Best practice methods for determining an electrode material's performance for ultracapacitors. *Energy Environ. Sci.* **3**, 1294–1301 (2010).

32. Zhang, J. & Zhao, X. S. On the configuration of supercapacitors for maximizing electrochemical performance. *ChemSusChem* **5**, 818–841 (2012).

33. Kim, T. Y. *et al.* High-performance supercapacitors based on poly(ionic liquid)-modified graphene electrodes. *ACS Nano* **5**, 436–442 (2011).

34. Denisa, H.-J. *et al.* Highly stable performance of supercapacitors from phosphorus-enriched carbons. *J. Am. Chem. Soc.* **131**, 5026–5027 (2009).

35. Liu, W., Yan, X., Lang, J., Peng, C. & Xue, Q. Flexible and conductive nanocomposite electrode based on graphene sheets and cotton cloth for supercapacitor. *J. Mater. Chem.* **22**, 17245–17253 (2012).

36. Chen, P.-C., Shen, G., Sukcharoenchoke, S. & Zhou, C. Flexible and transparent supercapacitor based on In_2O_3 nanowire/carbon nanotube heterogeneous films. *Appl. Phys. Lett.* **94**, 043113 (2009).

37. Taberna, P. L., Simon, P. & Fauvarque, J. F. Electrochemical characteristics and impedance spectroscopy studies of carbon-carbon supercapacitors. *J. Electrochem. Soc.* **150**, A292–A300 (2003).

38. Choi, B. G., Hong, J., Hong, W. H., Hammond, P. T. & Park, H. S. Facilitated ion transport in all-solid-state flexible supercapacitors. *ACS Nano* **5**, 7205–7213 (2011).

Acknowledgments

Author contributions

T.C. and L.D. designed experiments. T.C. carried out experiments and wrote the manuscript. T.C., H.P., M.D. and L.D. discussed the results and contributed to revision.

Additional information

Supplementary information accompanies this paper at http://www.nature.com/scientificreports

Competing financial interests: The authors declare no competing financial interests.

How to cite this article: Chen, T., Peng, H.S., Durstock, M. & Dai, L.M. High-performance transparent and stretchable all-solid supercapacitors based on highly aligned carbon nanotube sheets. *Sci. Rep.* **4**, 3612; DOI:10.1038/srep03612 (2014).